Scientific Journal for Damietta Faculty of Science **15**(2) 2025, 1-11
Doi: 10.21608/sjdfs.2025.383149.1230
ISSN Print 2314-8594
ISSN Online 2314-8616

https://sjdfs.journals.ekb.eg/

Quantum Chemical Molecular Dynamics and Experimental Studies of Corrosion Inhibition Effect of Allyl Rhodanine Azodye Derivatives on C-Steel in 2 M HCl

A.A. El-Sonbaty[*1], M. Mossad[2] and M.H. Mahmoud[1]

[1]Mathematical and Physical Engineering Department, Faculty of Engineering, Mansoura University, El-Mansoura, Egypt.
[2]Public Works Engineering Department, Faculty of Engineering, Mansoura University, Mansoura 35516, Egypt.

Received: 12 April 2025 /Accepted: 25 May 2025

[*]Corresponding author's E-mail: aaelsonbaty@hotmail.com

Abstract

The inhibition impact of freshly created allyl rhodanine azodye derivatives inhibitors **(1-3)** on C-steel and their adsorption patterns in 2 M HCl were investigated were investigated using weight reduction strategy, potentiodynamic polarization, electrochemical impedance spectroscopy (EIS), electrochemical frequency modulation (EFM) techniques, and scanning electron microscopy (SEM). The total resistance of the carbon corrosion process and inhibition efficiency of compounds **(1-3)** was increased with the increase of the inhibitor concentration. The corrosion rate reduced as the percentage of the compounds in the HCl solution increased, according to Tafel polarisation curves..

Keywords: Corrosion prevention, Tafel polarization, Quantum chemical molecular dynamics parameters, C-steel

Introduction

Owing to its superior mechanical attributes and affordable price, carbon steel (CS) is utilised in a large variety of usage in industry. It is typically utilized in construction and metal processing equipment, chemical processing, drums, heat exchangers, tanks, and maritime applications. In pickling, manufacturing scrubbing, and oil-well acidizing, rust is typically removed with acid solutions, which causes corrosion process on C-steel. Oxidation inhibitors are thus used to reduce or avoid corrosion as well as to defend against sudden metal breakdown and acid consumption, mainly in acidic conditions **(Morgan *et al.*, 2017)**.

Chemical oxidation inhibitors with molecules of S, N_2 and O_2 and heterocyclic structures can significantly decrease the likelihood of corrosion when only extremely little amounts are added and consider more efficient inhibitors. [1,2] The mechanism of inhibition based on that the hetero atoms such as N, O or S atoms on the metal's surface reduced the flow of corrosion products to the

metal surface by limiting the active sites and creating a physical border **(Abou-Dobara *et al*., 2019a; Diab *et al*., 2019a; Eldesoky *et al*., 2015; El-Sonbati *et al*., 2019a; El-Sonbati *et al*., 2022a)**.

The research the prevention of corrosion and the weight reduction technique, tafel polarisation, electrochemical impedance spectroscopy and electrochemistry frequency modulation methods were used to investigate the electrochemical performance of allyl rhodanine azodye derivatives inhibitors for C-steel in 2 M HCl solvent. The test coupon upper layer was examined using scanning electronic microscopy, which reported that these compounds avoided oxidation of C-steel in 2 M HCl by forming a shielding layer on its surface. That serves as a defence against corrosive environments.

Experimental

Molecular structure

Software called (Material Studio Version 4.4) has been used to do quantum chemical computations (Abou-Dobara *et al*., 2019b; Diab *et al*., 2018; El-Sonbati *et al*., 2018a; Mohamed *et al*., 2016; Refaat *et al*., 2016).

Composition of metal coupons and medium

C-steel, was employed for the oxidation examinations. Its weight percentage is 0.20 C, 0.30 Si, 0.53 Mn, 0.055S, 0.045 P, Fe balance. In order to create the test sample, which contains 2 M of HCl, HCl (BDH grade, 37%) was diluted with dual bidistilled water.

Inhibitor preparation and characterization

The inhibitors (Table 1) used for this study were derived from the reaction of N-allylrhodanine and p-aniline extracts bonding **(Abou-Dobara *et al*., 2019b; Diab *et al*., 2018; El-Sonbati *et al*., 2018a)**. The resulting s inhibitors were characterized and it was found that, compound **(1)**: brown solid, m.p. 185 ± 1 ºC, IR (KBr, υ cm^{-1}): 3444 (O–H), 1415 (N=N), 1727 (C=O), compound **(2)**: yellow solid, m.p. 178 ± 1 ºC, IR (KBr, υ cm^{-1}) 1490 (N=N), 1724 (C=O), and compound **(3)**: greenish yellow solid, m.p. 171 ± 1 ºC, IR (KBr, υ cm^{-1}) 1334 $(O–N=O)_{sy}$, 1496 $(O–N=O)_{Asy}$, 1554 (N=N), 1700 (C=O).

Table 1. Investigated inhibitors **(1-3)**.

Compound No.	
(1)	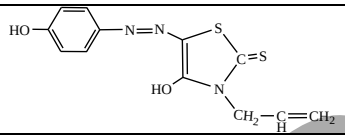
(2)	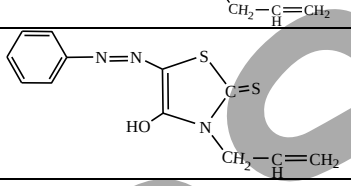
(3)	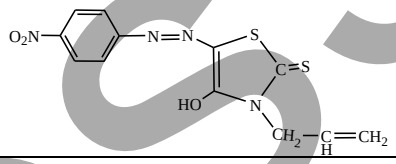

Measuring Methodologies

Weight reduction technique

Specimens of C-steel coupons as rectangular with dimensions 20.0 × 20.0 × 2 mm were rubbed with emery paper of varying grades; Triplicate Coupons were carried out for same behaviors with various temperatures. The corrosion proportion (υ) was estimated utilizing the formula (1):

$$\upsilon = W/St \qquad (1)$$

where W represents the three adjacent carbon steel coupons' approximate amount reduction, S is the amount of carbon steel coupons' surface and t is the exposure period. The evaluated chemicals' IE_w% protective effectiveness on the carbon steel oxidation was computed by equation (1):

$$IE_w\,\% = (\upsilon_\circ - \upsilon)/\upsilon_\circ \times 100 \qquad (1)$$

where υ_o and υ are the corrosion percentage readings before and after adding the inhibitor.

Tafel polarization technique

The electrochemical procedure was carried out **(Morgan *et al*., 2017)**.

Frequency Modulation by Electrochemistry procedure

The use of electrochemical modulation technique can be a nondestructive experiment and fast technique for measure the rate of corrosion.

Electrochemical impedance spectroscopy

The comparable electric connection modeling within the system uses R_{ct} to describe the charge transfer, R to indicate the resistor, R_s to reflect the solution resistance, and C_{dl} to represent the capacity of the dual layer.

Surface morphology

With and without the recommended dose of the examined inhibitors, the steel's analysis was submerged in one molar hydrochloric acid for 12 hours.

Results and discussion

Mass diminution method

As illustrated in Figure 1, the degradation of C-steel masses in 2 M HCl decreases approximately linearly as time without and with varying doses of compound **(1)** at 30 ± 1 ºC. Comparing the rate of corrosion to that without inhibitors IE_w % is computed using equation (2) **(Morgan *et al.*, 2017)**:

$$IE_w\% = 100 \times \left[1 - \left(C.R_{Corr}/C.R^{\circ}_{Corr}\right)\right] \quad (2)$$

where $C.R^{\circ}_{corr}$ and $C.R_{corr}$ are the corrosion rates without and with inhibitor, respectively. The (% IE_w) of the organic inhibitor derivatives listed in Table 1 obeyed the sequence: compound **(1)** > compound **(2)** > compound **(3)**. Straight line was obtained by plotting % IE against Hammett's substituent coefficients (σ^R) (Figure 2).

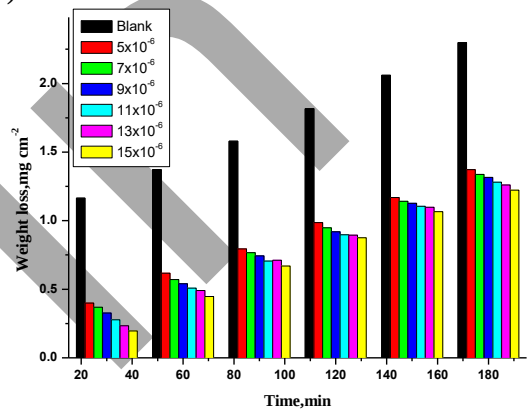

Figure 1. Charts demonstrating the mass-reduction of inhibitor **(1)**.

Table 2. Variation of indicators of losing the weight at 60 minutes.

Conc. (M)	Inhibition efficiency (%IE)		
	(1)	(2)	(3)
1×10^{-6}	55.0	49.0	37.7
3×10^{-6}	58.4	51.2	42.2
5×10^{-6}	60.7	54.3	45.0
7×10^{-6}	62.9	57.9	47.9
9×10^{-6}	64.2	59.8	51.7
11×10^{-6}	67.43	62.47	54.52

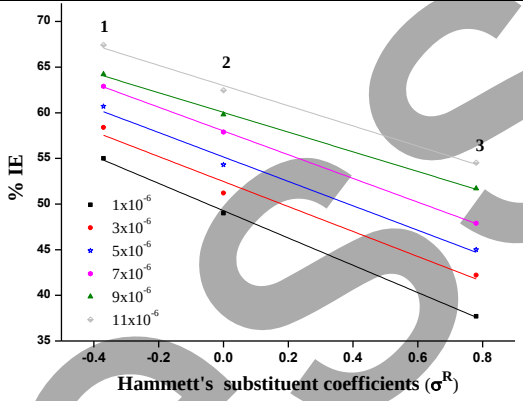

Figure 2. % IE against σ^R of the compounds.

Kinetic results

Using the formula: one can determine the Arrhenius activation energy (E_a*) value (Figure 3).

$$C.R = A\exp(-E_a^*/RT) \quad (3)$$

where A is the Arrhenius constant, T is the absolute temperature, k is the corrosion rate and R is the universal gas constant. According to Figure 3, the activation energy for carbon steel corrosion in 2 M HCl was determined to be 32 kJ mol^{-1}, which is consistent with the information obtained by other researchers **(Eldesoky *et al.*, 2015; El-Sonbati *et al.*, 2019a; El-Sonbati *et al.*, 2022a)**. Applying the transition condition theory using equation (4):

$$C.R = RT/Nh\, e^{(\Delta S^*/R)} e^{(-\Delta H^*/RT)} \quad (4)$$

Straight lines result from the draw of 1/T versus log k/T; since its interrupt and slope, ΔS* and ΔH* be able to be estimated, one-to-one (Figure 4 & Table 3). Equations were made to determine the activation enthalpy and entropy (ΔH* and ΔS*) of the corrosion process. Given that there is less disordering occurring as reactants go from the reactants to the activated compound, the -ve ΔS* signals point to an attachment stage rather than a dissociate stage being represented by the active site in the rate-determining stage. The endothermic nature of the metal dissolving process is shown in the +ve

ΔH* signs. [3-5]

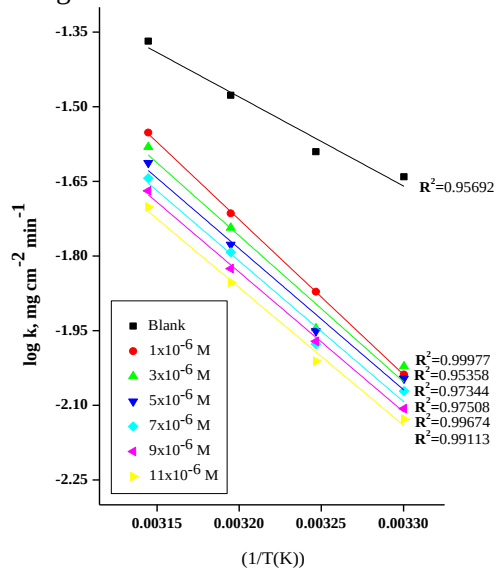

Figure 3. log k *vs.* 1/T curves for C-steel of inhibitor **(1)**.

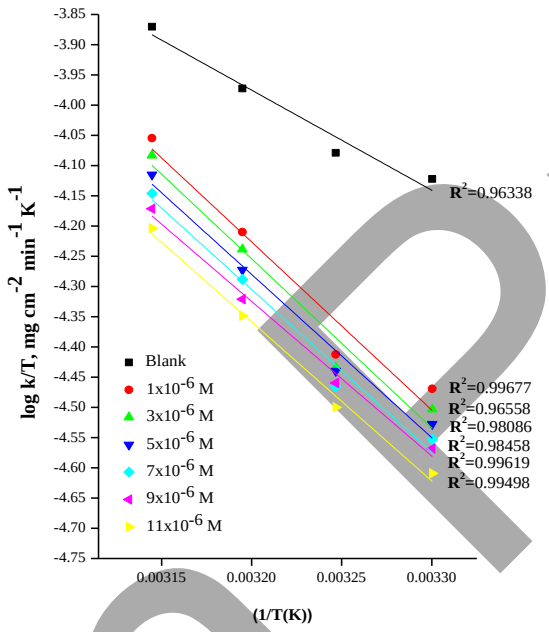

Figure 4. log (k /T) *vs.* 1/T curves for C-steel dissolution of inhibitor **(1)**.

Obviously, the activation energy (E^*_a) data using higher than when there are no inhibitors. Physical adsorption results from the increased E^*_a measurements when organic inhibitors are present among the surface of C-steel and inhibitors molecules. As a result, the E^*_a increment statistics result in a decreased corrosion rate.

Table 3. The dissolution Kinetic factors.

Comp.	Conc. (M)	E_a^* (kJ mol^{-1})	ΔH* (kJ mol^{-1})	-ΔS* (J mol^{-1} K^{-1})
Blank		34.285	30.572	175.81
(1)	1×10^{-6}	59.628	54.704	103.36
	3×10^{-6}	56.161	51.718	113.53
	5×10^{-6}	54.307	49.819	120.10
	7×10^{-6}	54.088	49.641	121.15
	9×10^{-6}	53.777	49.138	123.18
	11×10^{-6}	52.983	48.456	125.96
(2)	1×10^{-6}	48.365	43.922	137.06
	3×10^{-6}	49.020	44.551	135.35
	5×10^{-6}	51.294	46.737	128.71
	7×10^{-6}	54.061	49.386	120.65
	9×10^{-6}	53.943	52.033	112.63
	11×10^{-6}	57.863	53.014	110.52
(3)	1×10^{-6}	24.701	21.184	211.44
	3×10^{-6}	26.840	23.230	205.29
	5×10^{-6}	27.970	24.339	202.09
	7×10^{-6}	28.022	24.347	202.48
	9×10^{-6}	30.402	26.633	195.54
	11×10^{-6}	31.513	27.716	192.51

Theory for adsorption

The following equation (5) was used to calculate the various concentrations of the inhibitors of the carbon steel electrode.

$$\theta = \left[1 - \left(R_{corr}/R^{\circ}_{corr}\right)\right] \quad (5)$$

where R and R^o were used to illustrate the appropriate isotherm to evaluate the process adsorption. R and R^o were the rate of corrosion in hydrochloric acid as defined before and after at 30 ^{o}C: [4]

$$Org_{(sol)} + x(H_2O)_{ads} \leftrightarrow x(H_2O)_{(sol)} + Org_{(ads)} \quad (6)$$

Where x is the amount of water molecules that an inhibitor molecule replaces. Fitting (Θ) data to various isotherms has been attempted. According to the following equation (7), Temkin isotherm provided the best results for the adsorption data in the current study:

$$2a\theta = \ln(CK_{ads}) \quad (7)$$

Where a is the heterogeneous factor of the carbon steel surface, C is the dose of inhibitors and K_{ads} is the equilibrium constant for adsorption.

With the use of Kads, the Gibbs free adsorption energies (ΔG^o_{ads}) might be estimated as follows:

$$\Delta G^{\circ}_{ads} = -RT\ \ln(55.5\ K_{ads}) \quad (8)$$

where 55.5 is the concentration of 1L of water in solution (M/L).

If C is the bulk concentration of the inhibitor and 1/y is the number of surface- one inhibitor molecule's participation in the

effective spots, then K = K' (1/y) as following:

$$\log\left(\theta/(1-\theta)\right) = \log K' + y \log C \quad (9)$$

Table 4 contains the calculated values for K_{ads} and ΔG°_{ads}.

Table 4. The kinetic adsorption isotherm parameter after 60 minutes.

Inhibitors	K_{ads} (M^{-1})	$-\Delta G^{\circ}_{ads}$ (kJ mol^{-1})
(1)	1.317	10.813
(2)	1.265	10.712
(3)	1.233	10.647

According to the data in Table 4, the greater-efficiency inhibitor has higher - ve ΔG°_{ads} data, and the adsorption spontaneity for method and surface stabilization on the exterior of carbon steel. As a result, the following is the order of protective effectiveness: compound **(1)** follows compound **(2)**, and so on **(3)**. The data of K_{ads} were obtained to run in parallel to the IE [K **(1)** > K **(2)** > K **(3)**], and are affected by the substituent inductive or mesmeric effects. Figure 5 illustrates a straight line that results from charting the relationship between Hammett's substituent coefficients *vs.* K_{ads} and $-\Delta G^{\circ}_{ads}$ values.

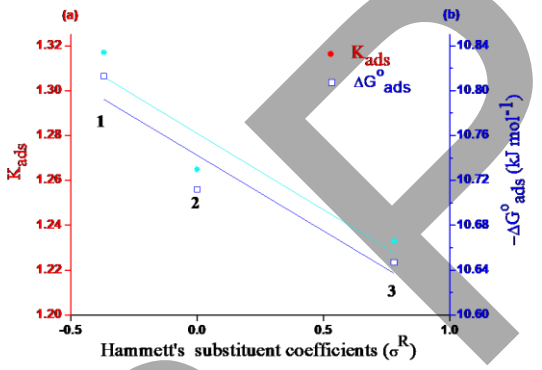

Figure 5. Hammett's substituent coefficients *vs.* K_{ads} and $-\Delta G^{\circ}_{ads}$

Tafel polarization measurements

By using the polarisation method, the impact of inhibitors on the corrosion of carbon steel was examined **(El-Sonbati *et al.*, 2019a; El-Sonbati *et al.*, 2022a)**. The Tafel polarization charts for carbon steel for different doses of chemical (1) at 25 °C are shown in Figure 6.

1. A reduction in the rate of corrosion, which causes a reduction in the current intensity (i_{corr})
2. An growth in the proportion of IE_p as a result of better covering surface

The corrosion potential values did not differ noticeably from the blank. Equation (10) was used to calculate the effectiveness of the inhibition:

$$\%\ IE_p = \left[\left(i^{\circ}_{corr} - i_{corr}\right)/i^{\circ}_{corr}\right] \times 100 \quad (10)$$

where i^{o}_{corr} and i_{corr} are, respectively, current corrosion flows without and with different amounts of compound **(1)**.

Table 5 shows that after the addition of the organic derivatives. The order of the effectiveness of inhibitors is: **(1)** > **(2)** > **(3)**.

Table 5. Kinetic characteristics.

Comp.	Conc., M.	$-E_{corr}$ (mV *vs.* SCE)	$\beta_a \times 10^{-3}$ (mV dec^{-1})	$\beta_c \times 10^{-3}$ (mV dec^{-1})	% IE
	Blank	**439**	**81.60**	**234.0**	**-----**
(1)	1×10^{-6}	477	88.90	166.8	80.5
	3×10^{-6}	467	91.70	214.5	80.6
	5×10^{-6}	478	100.20	158.1	81.1
	7×10^{-6}	489	83.60	188.1	81.3
	9×10^{-6}	482	49.40	91.7	93.7
	11×10^{-6}	466	36.70	63.9	96.0
(2)	1×10^{-6}	479	81.90	166.8	77.9
	3×10^{-6}	454	71.80	147.7	78.1
	5×10^{-6}	466	79.80	152.5	78.4
	7×10^{-6}	467	96.50	237.4	79.1
	9×10^{-6}	468	91.20	175.2	79.7
	11×10^{-6}	466	88.00	204.8	79.9
(3)	1×10^{-6}	439	78.10	215.4	5.7
	3×10^{-6}	467	113.50	232.2	50.3
	5×10^{-6}	453	74.30	158.2	61.5
	7×10^{-6}	479	89.00	152.7	75.7
	9×10^{-6}	467	79.70	147.1	76.3
	11×10^{-6}	480	106.40	155.4	76.8

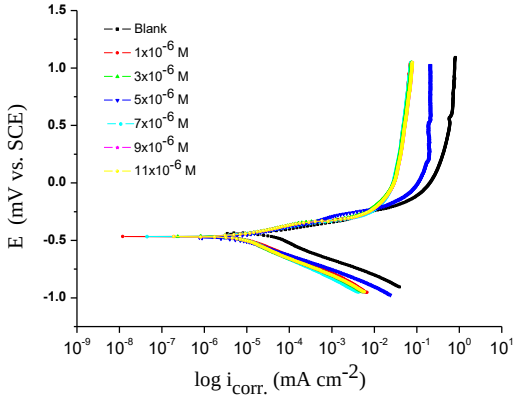

Figure 6. Potentiodynamic polarisation of inhibitor (1).

EFM methods

The optimum solution for online corrosion monitoring is provided by the EFM method. The EFM spectra for carbon steel containing and without distinct chemical (1) doses are shown in Figure 7. Table 6 includes the kinetic characteristics obtained

from EFM together with the causality variables (CF-2 and CF-3), corrosion density current (i_{corr}), cathodic and anodic Tafel lines (a and c), and corrosion density current (i_{corr}). The correlation factors CF-2 and CF-3, which are quite close to their theoretical values, show the high quality of the estimated values. Using equation 11, the inhibition efficiencies % IE_{EFM} were determined.

$$\% IE_{EFM} = \left[1 - \left(i_{corr}/i^{\circ}_{corr}\right)\right] \times 100 \quad (11)$$

where the terms i^{o}_{corr} and i_{corr} refer to the corrosion densities of both with and without them. This experiment's determination of protective efficiency is as follows:
(1) > (2) > (3).

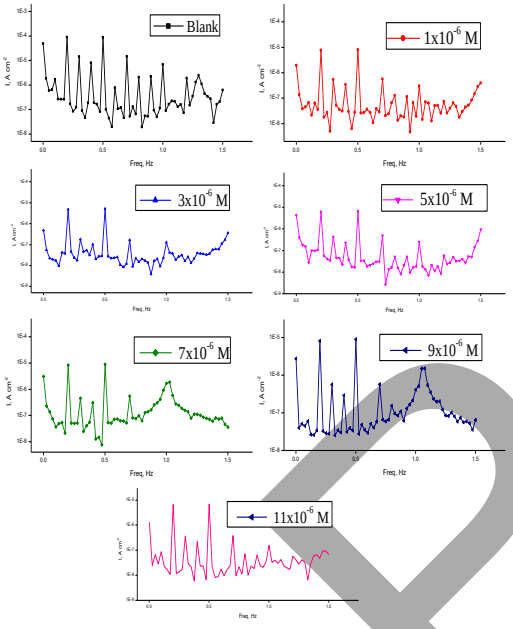

Figure 7. EFM spectra of compound **(1)**.

EIS evaluation

EIS is a potent and well-proven technology in the corrosion process. Impedance curves can be used to study kinetics of electrodes, surface properties, and mechanistic information. Figure 8 displays the (a) Nyquist and (b) Bode graphs minus and incorporating different dosages of inhibitors from open-circuit potential. This instruction was followed by the loop capacities increasing size (Figure 8a) in relation to a constant inhibitor dose: Compounds **(1)** through **(3)** demonstrate the higher inhibitory impact of compound **(1)**. Given the addition of the impedance increase caused by the addition of dosages of inhibitors, Bode curves (Figure 8b). This circuit, that depicts one electron transport reaction, is entirely according to the results of our experiments. For a circuit with a CPE variable (Y_0 and n), C_{dl} was determined by applying equation (12) **(Eldesoky *et al.*, 2015; Morgan *et al.*, 2017)**:

$$C_{dl} = Y^{\circ}\omega^{n-1}/\sin\left[n\left(\frac{\pi}{2}\right)\right] \quad (12)$$

where Y_0 = magnitude of the CPE, $\omega = 2\pi f_{max}$, at f_{max}, the imagined component of the impedance oscillates at its highest frequency. According to the results of the trials, charged transfer was mostly responsible for influencing the Nyquist charts for the corrosion reaction **(El-Sonbati *et al.*, 2019a; Morgan *et al.*, 2017)**.

Table 6. Electrochemical kinetic characteristics by the EFM

Comp.	Conc., M.	i_{corr} (μA cm^{-2})	$\beta_a \times 10^{-3}$ (mV dec^{-1})	$\beta_c \times 10^{-3}$ (mV dec^{-1})	CF-2	CF-3	%IE
	Blank	141.5	68.40	219.0	1.93	2.81	----
(1)	1×10^{-6}	16.11	172.2	272.6	2.05	3.02	88.6
	3×10^{-6}	15.78	116.5	236.6	1.92	3.21	88.8
	5×10^{-6}	14.53	90.94	134.3	2.03	2.98	89.7
	7×10^{-6}	13.62	85.48	131.8	1.82	2.54	90.3
	9×10^{-6}	13.50	90.68	149.1	1.69	2.95	90.4
	11×10^{-6}	12.62	99.56	150.5	1.97	2.83	91.0
(2)	1×10^{-6}	19.72	90.63	191.2	1.89	3.00	86.0
	3×10^{-6}	18.45	112.70	189.1	1.96	2.89	86.9
	5×10^{-6}	18.27	80.63	133.0	1.85	3.29	87.0
	7×10^{-6}	18.00	109.70	180.7	2.00	3.04	87.2
	9×10^{-6}	17.74	112.30	212.5	1.89	3.07	87.4
	11×10^{-6}	16.79	61.56	97.89	1.57	2.78	88.1
(3)	1×10^{-6}	49.38	80.64	194.7	1.90	2.91	65.1
	3×10^{-6}	31.64	88.90	180.7	1.89	3.40	77.6
	5×10^{-6}	25.46	76.70	135.0	1.93	2.90	82.0
	7×10^{-6}	24.01	115.50	242.2	1.95	2.88	83.0
	9×10^{-6}	22.28	87.63	167.6	1.88	3.04	84.2
	11×10^{-6}	21.92	138.20	211.7	1.99	2.69	84.5

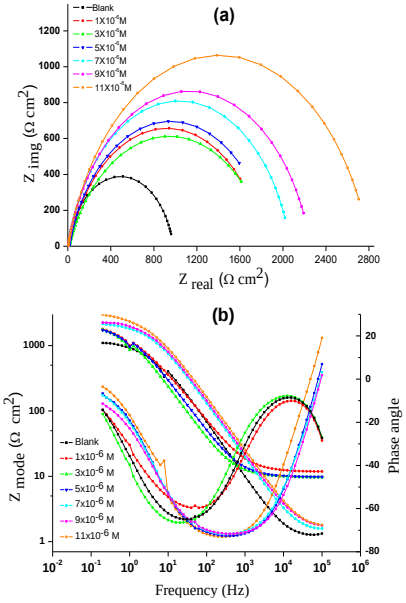

Figure 8. The Nyquist and Bode curves (a) and (b), respectively of compound **(1)**.

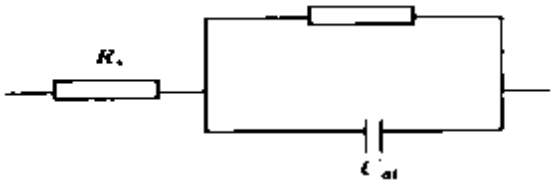

Figure 9. A model of an equivalent circuit is.

According to the EIS data in Table 7, when the concentrations of inhibitors increased, the R_{ct} data increased and as a result of the inhibitors sticking to the carbon steel's surface and the amount of the dissolving reaction was reduced, the C_{dl} data decreased. In general, an increase in R_{ct} data is accompanied by a decrease in corrosion, A decrease in C_{dl} could be caused by a rise in the thickness of electrical double layers or a fall in the local dielectric constant **(Moretti *et al.*, 1994)**.

$$\% E = \theta \times 100 = \left[1 - \left(R^{\circ}_{ct}/R_{ct}\right)\right] \quad (13)$$

where R^{o}_{ct} and R_{ct} refer for, respectively, the resistance to charge transfer with and without an inhibitor. Tafel polarization fits the percent %E order of the studied compounds (**1** > **2** > **3**).

Table 7. Data on the EIS.

Comp.	Conc., M.	R_S (Ω cm^2)	R_{ct} (Ω cm^2)	$C_{dl} \times 10^{-4}$ (μFcm^{-2})	% IE
	Blank	1.19	980	9.07	---
(1)	1×10^{-6}	9.44	1825	1.76	46.3
	3×10^{-6}	11.01	1862	1.73	47.3
	5×10^{-6}	9.50	1892	1.52	48.2
	7×10^{-6}	1.47	2070	1.37	52.6
	9×10^{-6}	1.67	2258	1.02	56.5
	11×10^{-6}	1.62	2803	1.01	65.0
(2)	1×10^{-6}	10.35	1635	2.64	40.0
	3×10^{-6}	9.96	1694	2.60	42.1
	5×10^{-6}	9.89	1739	2.52	43.6
	7×10^{-6}	1.36	1777	2.07	44.7
	9×10^{-6}	10.15	1778	1.81	44.8
	11×10^{-6}	1.34	1779	1.77	44.9
(3)	1×10^{-6}	11.81	1013	7.72	3.2
	3×10^{-6}	11.08	1253	3.48	21.7
	5×10^{-6}	1.11	1375	3.47	28.7
	7×10^{-6}	9.87	1455	2.97	32.6
	9×10^{-6}	14.11	1495	2.88	34.4
	11×10^{-6}	9.92	1580	2.73	37.9

SEM investigation and EDX analysis

The surfaces of carbon steel were examined using SEM prior to and after corrosion in 2 M HCl in the absence and existence of 11×10^{-6} M inhibitors as shown in Figure 10.

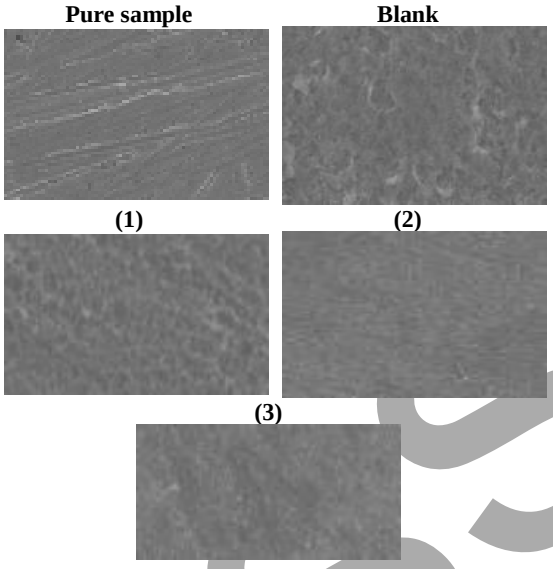

Figure 10. Carbon steel SEM micrographs

When carbon steel was exposed to 11×10^{-6} M of the examined inhibitors for three days, Figure 11 depicts the EDX spectrum of a surface made of carbon steel. A comparable distribution elemental is given in Table 8.

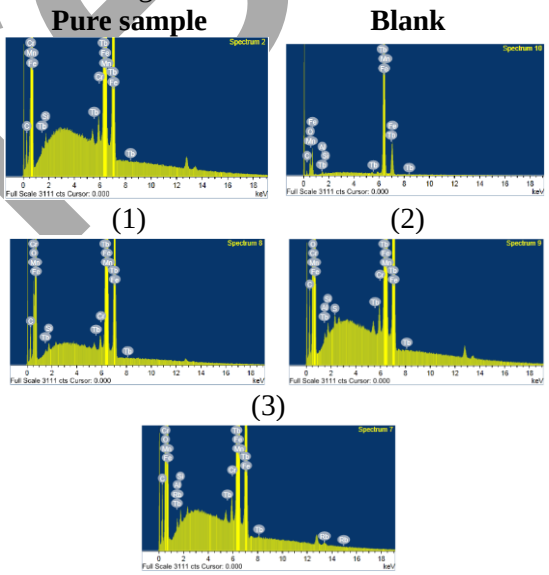

Figure 11. EDX study for CS containing.

Table 8. Composition of the surface.

Mass %	C	O	Al	Mn	Fe	S
Pure sample	6.78	---	0.29	0.47	87.53	---
Blank	10.58	14.84	0.70	0.40	69.75	---
(1)	10.83	12.02	0.31	0.45	71.51	---
(2)	11.14	9.15	0.19	0.47	74.40	0.17
(3)	11.45	7.41	---	0.43	76.47	---

Quantum chemical

Table 9 represents the calculation of a few quantum properties of the substances under

consideration in its keto form. Optimal geometries, HOMO distribution, and Figure 12 display the non-protonated LUMO distribution derivatives **(Diab *et al*., 2019b; El-Ghamaz *et al*., 2012; El-Sonbati *et al*., 2018b; El-Sonbati *et al*., 2018c; El-Sonbati *et al*., 2022b; Morgan *et al*., 2018; Salama *et al*., 2023)**. As a result, inhibitor molecules can receive electrons from the metal more readily the lesser the LUMO potential. As a result, the energy band gap value, $\Delta E = E_{LUMO} - E_{HOMO}$, reflects the inhibitor's ability to stop reactions; the smaller its value, the greater the effectiveness of the inhibition **(Diab *et al*., 2019c; Diab *et al*., 2022; El-Sonbati *et al*., 2018d; El-Sonbati *et al*., 2019b; El- El-Sonbati *et al*., 2020; El-Sonbati *et al*., 2021)**. Compound 1 has the most E_{HOMO}, followed by compound **(2)** and compound **(3)**, due to the presence existence of an electron-donating group (OH) in its molecular structure.

Table 9. The estimated quantum chemical characteristics.

	(1)	**(2)**	**(3)**
E_{HOMO} (eV)	-3.363	-3.333	-5.832
E_{LUMO} (eV)	-2.948	-2.352	-3.303
ΔE (eV)	0.415	0.981	2.529
η (eV)	3.156	2.843	4.568
σ (eV^{-1})	0.208	0.491	1.265
Pi (eV)	-4.819	-2.039	-0.791
S (eV^{-1})	2.409	1.0194	0.395
ω (eV)	23.993	8.236	8.249
ΔN_{max}	15.207	5.795	3.612

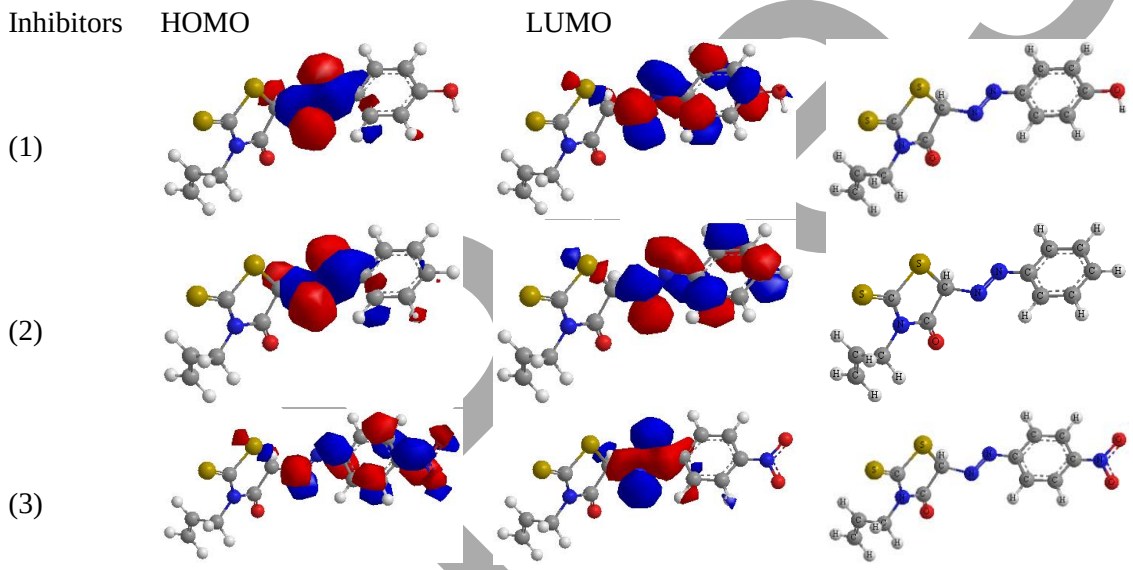

Figure 12. Molecular orbital plots.

Compound **(1)** has a strong tendency to donate electrons. Additionally, compound **(1)** has a lesser E_{LUMO} value, which confirms compound stronger corrosion behavior **(1)**. Another evidence for compound **(1)** stronger propensity to adsorb onto the surface of carbon steel comes from the fact that it has a lower ΔE value.

Conclusions

1. All of the studied chemicals are found to be effective carbon steel corrosion inhibitors in 2 M HCl solution.
2. The kind and variety of substituents found in the inhibitor molecule determine the various levels of inhibitive activity.
3. EFM was utilized as a quick and non-destructive method to measure corrosion. Adding the inhibitor increased the resistance to charge transfer and decreased the double layer capacitances, raising the IE percentage, according to the EIS data.
4. Allyl rhodanine azodye compounds are mixed-type inhibitors, according to the results of potentiodynamic polarization.
5. SEM-EDX pictures and analysis showed that a thin layer had formed on the carbon steel. The results of the electrochemical and chemical

investigations were in good agreement.

6. The active sites of the derivatives of allyl rhodanine and azodye were determined by quantum chemistry calculations to be hetero atoms of both oxygen and nitrogen **(1-3)**.

Highlights:

The inhibition impact of freshly created allyl rhodanine azodye derivatives **(1-3)** on C-steel (CS) and their adsorption patterns in 2M HCl were investigated.

The corrosion rate reduced as the percentage of the compounds in the HCl solution increased, according to Tafel polarisation curves. On corrosion inhibition process, the temperature effect has been studied.

References

Abou-Dobara MI, Omar NF, Diab, MA, El-Sonbati AZ, Morgan ShM, Salem OL, Eldesoky AM. 2019a. Polymer complexes. LXXV. Characterization of quinoline polymer complexes as potential bio-active and anti-corrosion agents. Mater. Sci. Eng. C., 103, 109727. https://doi.org/10.1016/j.msec.2019.05.012

Abou-Dobara MI, Omar NF, Diab MA, El-Sonbati AZ, Morgan ShM, El-Mogazy MA. 2019b. Allyl rhodanine azo dye derivatives: Potential antimicrobials target d-alanyl carrier protein ligase and nucleoside diphosphate kinase. J. Cell. Biochem., 120(2), 1667-1678. https://doi.org/10.1002/jcb.27473

Diab MA, El-Sonbati AZ, Morgan ShM, El-Mogazy MA. 2018. Polymer complexes. LXXI. Spectroscopic studies, thermal properties, DNA binding and antimicrobial activity of polymer complexes. Appl. Organomet. Chem., 32(8), e4378. https://doi.org/10.1002/aoc.4378

Diab MA, Nozha SG, El-Sonbati AZ, El-Mogazy MA, Morgan ShM. 2019a. Polymer complexes. LXXVIII. Synthesis and characterization of supramolecular uranyl polymer complexes: Determination of the bond lengths of uranyl ion in polymer complexes. Appl. Organomet. Chem., 33(10), e5153. https://doi.org/10.1002/aoc.5153

Diab MA, El-Sonbati AZ, El-Ghamaz NA, Morgan ShM, El-Shahat O. 2019b. Conducting polymers X: Dielectric constant, conduction mechanism and correlation between theoretical parameters and electrical conductivity of poly (N, N′-bis-sulphinyl p-phenylenediamine-2, 6-diaminipyridine) and poly (N, N′-bis-sulphinyl p-phenylenediamine-3, 5-diamine-1, 2, 4-trizole). Eur. Polym. J., 115, 268-281. https://doi.org/10.1016/j.eurpolymj.2019.03.036

Diab MA, Mohamed GG, Mahmoud WH, El-Sonbati AZ, Morgan ShM, Abbas SY. 2019c. Inner metal complexes of tetradentate Schiff base: Synthesis, characterization, biological activity and molecular docking studies. Appl. Organomet. Chem., 33(7), e4945. https://doi.org/10.1002/aoc.4945

Diab MA, El-Sonbati AZ, Gomaa EA, El-Mogazy MA, Morgan ShM, Abou-Dobara MI, Osman MA. 2022. Polymer complexes: LXXIX—synthesis, characterization, geometrical structures, biological activity and molecular docking studies of azo dye complexes. J. Iran. Chem. Soc., 19(7), 3079-3102. https://doi.org/10.1007/s13738-022-02516-9

Eldesoky AM, El-Bindary MA, El-Sonbati AZ, Morgan ShM. 2015. New eco-friendly corrosion inhibitors based on azo rhodanine derivatives for protection copper corrosion. J. Mater. Environ. Sci., 6, 2260-76. https://ksascholar.dri.sa/en/publications/new-eco-friendly-corrosion-inhibitors-based-on-azo-rhodanine-deri

El-Ghamaz NA, El-Sonbati AZ, Morgan ShM. 2012. Optical properties of some synthesized azo thin films. J. Mol. Struct., 1027, 92-98. https://doi.org/10.1016/j.molstruc.2012.06.004

El-Sonbati AZ, Diab MA, Morgan ShM, El-Mogazy MA. 2018a. Polymer complexes. LXXIII. Synthesis, characterization, thermal properties, electron spin resonance study and antimicrobial activity of Cu (II) polymer complexes: Relation between representative Pascal constants and thermal activation energy of decomposition. Appl. Organomet. Chem., 32(11), e4530. https://doi.org/10.1002/aoc.4530

El-Sonbati AZ, Diab MA, Morgan ShM, Eldesoky AM, Balboula MZ. 2018b. Polymer complexes. LXIX. Some divalent metal (II) polymer complexes of potentially bidentate monomer N-[4-(5-methyl-isoxazol-3-ylsulfamoyl)-phenyl]-acrylamide: synthesis, spectroscopic characterization, thermal properties, antimicrobial agents and DNA studies. Appl. Organomet. Chem., 32(3), e4207. https://doi.org/10.1002/aoc.4207

El-Sonbati AZ, Diab MA, Morgan ShM, Balboula MZ. 2018c. Polymer complexes. LXVIII. Spectroscopic studies of supramolecular copper (II) polymeric complexes of biologically active monomer derived from novel sulfa drug. Appl. Organomet. Chem., 32(2), e4059. https://doi.org/10.1002/aoc.4059

El-Sonbati AZ, Diab MA, Morgan ShM, Seyam HA. 2018d. Supramolecular structures for determination and identification of the bond lengths in novel uranyl complexes from their infrared spectra. J. Mol. Struct., 1154, 354-365. https://doi.org/10.1016/j.molstruc.2017.10.020

El-Sonbati AZ, Diab MA, Eldesoky AM, Morgan ShM, Salem OL. 2019a. Polymer complexes. LXXVI. Synthesis, characterization, CT-DNA binding, molecular docking and thermal studies of sulfoxine polymer complexes. Appl. Organomet. Chem., 33(5), e4839. https://doi.org/10.1002/aoc.4839

El-Sonbati AZ, Mahmoud WH, Mohamed GG, Diab MA, Morgan ShM, Abbas SY. 2019b. Synthesis, characterization of Schiff base metal complexes and their biological investigation. Appl. Organomet. Chem., 33(9), e5048. https://doi.org/10.1002/aoc.5048

El-Sonbati AZ, Diab MA, Morgan ShM, Abou-Dobara MI, El-Ghettany AA. 2020. Synthesis, characterization, theoretical and molecular docking studies of mixed-ligand complexes of Cu (II), Ni (II), Co (II), Mn (II), Cr (III), UO2 (II) and Cd (II). J. Mol. Struct., 1200, 127065. https://doi.org/10.1016/j.molstruc.2019.127065

El-Sonbati AZ, Omar NF, Abou-Dobara MI, Diab MA, El-Mogazy MA, Morgan ShM, El-Ghettany AA. 2021. Structural, molecular docking computational studies and in-vitro evidence for antibacterial activity of mixed ligand complexes. J. Mol. Struct., 1239, 130481. https://doi.org/10.1016/j.molstruc.2021.130481

El-Sonbati AZ, El-Mogazy MA, Nozha SG, Diab MA, Abou-Dobara MI, Eldesoky AM, Morgan ShM. 2022a. Mixed ligand transition metal (II) complexes: Characterization, spectral, electrochemical studies, molecular docking and bacteriological application. J. Mol. Struct., 1248, 131498. https://doi.org/10.1016/j.molstruc.2021.131498

El-Sonbati AZ, Diab MA, Morgan ShM, Abbas SY, Mohamed GG. 2022b. Synthesis, theoretical study, molecular docking and biological activity of nano tridentate (E)-2-((3-hydoxyphenyl) methyl) phenol metal complexes. Inorg. Chem. Commun., 137, 109193. https://doi.org/10.1016/j.inoche.2022.109193

Mohamed GG, El-Sherif AA, Saad MA, El-Sawy SE, Morgan ShM. 2016. Mixed-ligand complex formation of tenoxicam drug with some transition metal ions in presence of valine: Synthesis, characterization, molecular docking, potentiometric and evaluation of the humeral immune response of calves. J. Mol. Liq., 223, 1311-1332. https://doi.org/10.1016/j.molliq.2016.09.065

Moretti G, Quartanone G, Tassan A, Zingales A. 1994. Inhibition of mild steel corrosion in 1N sulphuric acid through indole. Werkst. Korros., 45(12), 641-647. https://doi.org/10.1002/maco.19940451203

Morgan ShM, El-Sonbati AZ, Eissa HR. 2017. Geometrical structures, thermal properties and spectroscopic studies of Schiff base complexes: Correlation between ionic radius of metal complexes and DNA binding. Mol. Liq., 240, 752-776. http://dx.doi.org/10.1016/j.molliq.2017.05.114

Morgan ShM, Diab MA, El-Sonbati AZ. 2018. Supramolecular assembly of hydrogen bonding, ESR studies and theoretical calculations of Cu (II) complexes. Appl. Organomet. Chem., 32(10), e4504. https://doi.org/10.1002/aoc.4504

Salama HM, Diab MA, El-Sonbati AZ, El-Mogazy MA, Eldesoky AM, Amin BH, El-Zahed MM. 2023. New potential Mn (II) mixed ligand complexes: synthesis, structural characterization, molecular docking, antibacterial activity and electrochemical studies. JICS, 20(12), 2977-3007. https://doi.org/10.1007/s13738-023-02892-w

Refaat HM, El-Badway HA, Morgan ShM. 2016. Molecular docking, geometrical structure, potentiometric and thermodynamic studies of moxifloxacin and its metal complexes. J. Mol. Liq., 220, 802-812. https://doi.org/10.1016/j.molliq.2016.04.124

الملخص العربي

عنوان البحث: الديناميكيات الجزيئية الكيميائية الكمية والدراسات التجريبية لتأثير تثبيط التآكل لمشتقات أزوداي الأليل رودانين على الفولاذ الكربوني في ٢ مولر حمض الهيدروكلوريك

أحمد السنباطي[١]، محمد مسعد[٢]، محمد حنفي محمود[١]

[١]قسم الهندسة الرياضية والفيزيائية، كلية الهندسة، جامعة المنصورة، المنصورة، مصر

[٢] قسم هندسة الأشغال العامة، كلية الهندسة، جامعة المنصورة، المنصورة، مصر

يشتمل البحث علي دراسة تآكل الصلب الكربونى في محلول ٢ مولر من حمض الهيدروكلوريك في عدم وجود وفي وجود لمشتقات أزوداي الأليل رودانين باستخدام طرق الفقد في الوزن والاستقطاب المهبطى والمصعدى وتقنيات المعاوقة الكهروكيميائية الطيفية ((EISوالتردد الكهروكيميائي المعدل (EFM)حيث وجد أن هذه المركبات تقلل من تآكل الصلب الكربونى. كذلك وجد أن معدل التآكل يزداد بزيادة درجة الحرارة وأن التثبيط يحدث عن طريق ادمصاص فيزيائي. واظهرت النتائج تطابقا تاما في جميع التقنيات المستخدمة. ووجد أن كفاءة التثبيط للمركبات كانت كالتالى:

(1) > (2) > (3)

.